Metallomics

Metallomic and Lipidomic Analysis of *S. cerevisiae* Response to Cellulosic Copper Nanoparticles Uncover Drivers of Toxicity

Journal:	*Metallomics*
Manuscript ID	MT-ART-01-2020-000018.R1
Article Type:	Paper
Date Submitted by the Author:	01-Mar-2020
Complete List of Authors:	Winans, Matthew; West Virginia University, Biology Gallagher, Jennifer; West Virginia University, Biology

Significance to Metallomics

Approximately one-third of all proteins and half of all enzymes are predicted to be dependent on a metal ion for structure or function. Proteomic and genetic analysis demonstrate a link between copper and zinc homeostasis. Cellulosic copper nanoparticles are uniquely toxic compared to soluble copper sulfate. The physical, chemical and functional properties of particles on the nanometer scale often differ from their dissolved or larger particle counterparts of the same elemental species This study elucidates the understanding of the metallome, metabolome, and the mechanistic drivers during the exposure of carboxymethylcellulose copper nanoparticles.

Metallomic and Lipidomic Analysis of *S. cerevisiae* Response to Cellulosic Copper Nanoparticles Uncover Drivers of Toxicity

Matthew J. Winans and Jennifer E. G. Gallagher*
West Virginia University – Biology Department, 53 Campus Drive LSB 3140, Morgantown, WV, 26506

*Corresponding Author: Jennifer E. G. Gallagher

Keywords: copper, metal, nano, nanotoxicity, nanoparticle, ROS, yeast, lipid, membrane, damage, CMC, carboxymethyl cellulose, cellulose, nanotechnology, antimicrobial, metabolomics, electron microscopy,

Abstract

Nanotechnology is a promising new technology, of which antimicrobial metal nanocomposites are predicted to become valuable in medical and food packaging applications. Copper is a redox-active antimicrobial metal that can become increasingly toxic depending on the target biomolecule's donor atom selectivity and the chemical species of copper present. Mass is the traditional measurement of the intrinsic elemental chemistry, but this practice fails to reflect the morphology and surface area reactivity of nanotechnology. The carboxymethyl cellulose copper nanoparticles (CMC-Cu) investigated in this study have unique and undefined toxicity to *Saccharomyces cerevisiae* that is different from $CuSO_4$. Cellular surface damage was found in scanning electron micrographs upon CMC-Cu exposure. Further investigation into the lipids revealed altered phosphatidylcholine and phosphatidylethanolamine membrane composition, as well as depleted triacylglycerols, suggesting an impact on the Kennedy lipid pathway. High levels of reactive oxygen species were measured which likely played a role in the lipid peroxidation detected with CMC-Cu treatment. Metal homeostasis was affected by CMC-Cu treatment. The copper sensitive yeast strain, YJM789, significantly decreased cellular zinc concentrations while the copper concentrations increased, suggesting a possible ionic mimicry relationship. In contrast to other compounds that generate ROS, no evidence of genotoxicity was found. As commonplace objects become more integrated with nanotechnology, humanity must look forward past traditional measurements of toxicity.

Significance to Metallomics

Approximately one-third of all proteins and half of all enzymes are predicted to be dependent on a metal ion for structure or function. Copper and zinc homeostasis have mounting proteomic and genetic evidence that suggests a link between the two metals. Cellulosic copper nanoparticles are uniquely toxic compared to soluble copper sulfate. The physical, chemical and functional properties of particles on the nanometer scale often differ from their dissolved or larger particle counterparts of the same elemental species. This study elucidates the understanding of the metallome, metabolome, and mechanistic drivers during the exposure of carboxymethylcellulose copper nanoparticles.

Introduction

Copper is known as a broad-spectrum biocidal towards microorganisms[1–3]. Since antiquity, copper vessels have been used for disinfection of water and preservation of food against microrganisms[4], yet humans have a low contact sensitivity from coinage and personal adornment[5]. In general, antimicrobial metals selectively disrupt cell growth. This growth disruption is influenced by the properties of both the metal and the available donor ligands on any biomolecules affected. This antimicrobial metal species damage is spatially localized disrupting membrane function, causing dysfunctional proteins, and DNA damage[6]. Important determinants of metal antimicrobial toxicity are donor atom selectivity, speciation, and reduction potential[2,6]. Donor atom selectivity is a factor that influences the compatibility between metal and the ligand that is potentially damaged. Speciation is important because the species of metal has a large influence on its bioavailability and reduction potential, for instance, the difference between Cu^{1+} and Cu^{2+}[7,8]. Moreover, potentially toxic materials have several driving factors including their intrinsic chemistry, surface area reactivity, and morphology; which influence any material's interaction with organisms.

Transition metals, particularly copper and iron, are two that are well known to be reduction-oxidation (redox)-active, but not all metals are active this way. This critically impacts their toxicity because redox-active metals sequentially reduce oxygen through the addition of electrons, forming reactive oxygen species (ROS). In biological systems, finely tuned redox activity facilitates the gain or loss of electrons between two chemical species enabling fundamental processes such as respiration, nitrogen fixation, and photosynthesis[9]. During cellular respiration, the mitochondria produce endogenous ROS as a result of oxygen reduction. This is a consequence of electrons being transferred between complexes to generate an electron potential across the mitochondrial membrane, generating ATP. H_2O_2 and $\cdot^{-}O_2$ are products of transferring electrons to molecular oxygen and progenitors of ROS[10]. In addition to molecule damage, it is well established that ROS can also act as a signaling molecule throughout the cell triggering cell signaling proteins, transporters, ion channels, modifying protein kinase, and ubiquitination systems[11]. A major mechanism of coppers toxicity to microorganisms is the disruption of the plasma membrane's integrity in which the fatty acid composition directly affects their susceptibility to copper in *S. cerevisiae*[12]. There is limited research on copper's influence on lipid biology, but copper ions have been shown to interact with synthetic membrane models of phosphatidylcholine (PC) and phosphatidylethanolamine (PE) in an ordered fashion. PC interacts with copper before PE based on the structure of the membrane prevalent phospholipids[13].

Aqueous copper exists in the particulate, colloidal, nanoparticle, and soluble states, predominately as metal and Cu^{2+} ions[6,14]. Inside the cell, essential metals are almost never free because of a plethora of transporters, regulatory sensors, and chaperones that confine the metal species and guide metal atoms to specific sites in proteins[9]. Interactions of metal ions with the atoms of ligand donors, such as functional groups of proteins, are strongly selective[15,16] and have a bias that facilitates the recognition of correct metal[17]. Approximately one-third of all proteins and half of all enzymes are predicted to be dependent on a metal ion for structure or function[17–19]. Proteins have a somewhat flexible steric selection for their desired metal and their selection is predisposed by an ordered universal preference for essential divalent cations such as copper over zinc[20]. Copper is the third most biologically abundant transition metal after iron and zinc, and unbalanced metal homeostasis results in the mis-metallation of proteins[21]. When metal homeostasis is unbalanced

some proteins bind incorrect metals, negatively influencing their structure and function. Lowly discriminate biomolecules contribute to ionic or molecular mimicry by binding with metal ions or metal complexes that resemble their correct cofactors[2]. Co-transportation of metals with ligands has also been shown to be a source of metal accumulation[22]. Yeast cells accumulate surplus metals in vacuoles[23,24] and intracellular accumulation of metal is routinely the first step in metal poisoning[6].

The CMC-Cu nanomaterials are considered a hybrid material, composed of copper nanoparticles and cellulose. It is a fibrous, hardy, water-insoluble substance composed of a high molecular weight homopolymer of β-1,4-linked anhydro-D-glucose units that maintain the structure of cell walls in plants[25]. The high number of Na-carboxyl groups on carboxymethyl (CMC) make it an attractive organic support structure on which to construct copper nanoparticles because it can facilitate copper's reduction and therefore further copper's availability on the cellulose structure[26,27]. They are synthesized *in situ* and reduced onto available carboxylic groups of carboxymethyl cellulose (CMC) as a template and stabilizer in order to manufacture nanocomposite materials[27]. These CMC microfibril strands contain the reduced copper nanoparticles (CuNP) that exhibit mostly Cu^{1+} and Cu^{0} forms averaging 15 nm in diameter[27]. CuNPs are built on CMC, forming CMC-Cu. Copper is thought to be slowly released as Cu(I) and then oxidized making Cu(II) available to interact with biological molecules leading to an intrinsic toxicity[28]. Variations in the copper composition and cellulose biopolymer have been successfully synthesized resulting in changes to their interaction with microorganisms[29–32]. CMC-Cu sensitivity mirrors the sensitivity of genetically diverse yeast exposed to soluble copper in $CuSO_4$ form[28]. When copper oxide is presented to yeast on the nanoscale, it is approximately 60-fold more toxic than its soluble counterpart[33]. Earlier work established that the derivative of cellulose and how the microorganisms were exposed, whether in liquid or what material the CMC-Cu was embedded in, made a difference in the kinetic and biological reaction[30]. Previous studies in higher eukaryotes found that CuO NPs have a "Trojan horse mechanism" that induces endocytosis and causes DNA damage by the intracellular ionic release of copper[34]. CuNPs appear to target the cell membrane to cause cellular death by loss of membrane integrity[35].

This study builds upon the proteomic and genetic evidence found in the first exposures of CMC-Cu to *S. cerevisiae*[28] by furthering the toxicological profile of the cellular response to include the metallomic and metabolomic aspects. Mounting evidence lead to the hypothesis that lipid interaction of the cellular membrane is the primary process by which CMC-Cu impart their nanotoxicity. These findings align with previous reports suggesting that copper causes a loss in the cellular membrane's integrity[6,36]. Copper nanoparticles derived from CMC-Cu treatments decrease cellular viability, which unlike soluble copper sulfate, is rescued by glutathione, but not its precursor N-acetylcysteine (NAC)[28]. This is indicative of the exogenous nature of CMC-Cu's primary nanotoxicological process. This original research investigated the influence of CMC-Cu exposures to *S. cerevisiae* on metal homeostasis, ROS production, lipid interaction, cellular morphology, and genotoxicity.

Methods and Materials

Yeast Growth and Treatment Conditions

All *S. cerevisiae* yeast strains were grown in either YPD (yeast rich media, 1% yeast extract, 2% peptone, 2% dextrose) or YM (yeast minimal media, 0.67% yeast nitrogen base without amino acids, 2% dextrose) supplemented with amino acids needed to complement any auxotrophic markers (histidine, uracil, leucine, and methionine (HULM) or lysine (HULK)). Yeast strains were maintained indefinitely at -80ºC in a 15% glycerol solution, temporarily at 4ºC on solid YPD or YM agar plates, and readily by log-phase growth at 30ºC in YPD or YM liquid media. Growth was measured by optical density at 600nm.

Yeast were treated with soluble copper at 400 μM by copper sulfate addition. Yeast were treated with copper nanoparticles at 157 μM copper by CMC-Cu addition. Glutathione (GSH) was supplied at 4.16 mM in the media. The concentration of CMC in both the CMC-Cu and CMC was 10 μg mL^{-1}. Exposure of 157 μM copper in NPs is effective as 400 μM copper sulfate in inhibiting the growth of YJM789, the copper sensitive strain[28]. These growth and treatment conditions were used to highlight the increase in toxicity from the enhanced delivery of Cu to the cytoplasm.

Cellular Metals

Yeast strains BY4741 and YJM789 were grown in triplicate until log-phase in YM+HULM (histidine, uracil, leucine, and methionine) or YM at 30°C, respectively. Yeast cells were treated with 400 μM CuSO4 or 157 μM CMC-Cu for 90 minutes. An equal number of cells were determined by optical density at 600 nm to collect equivalent to 5 optical density units (ODu) of cells. These samples were centrifuged and washed twice with distilled water. One ODu was separated for protein quantification. Samples were split, frozen in liquid nitrogen, and stored at -80°C. Soluble protein concentration was determined via Bradford assay as previously published [28]. For inductively coupled plasma – optical emission spectroscopy (ICP-OES), the cell pellets were treated with 600 μL of concentrated HNO_3 and 200 μL of 30% H_2O_2 for digestion[37]. These solutions were transferred to glass tubes and placed in a boiling water bath for 2 hours until clear. The liquids were filtered via syringe and readjusted to their original volumes with distilled water. Samples were analyzed at 327.395 nm for Cu and at 213.857 nm for Zn. Metal concentrations were given in mg ml^{-1} and normalized to soluble protein concentration for each sample. Three biological replicates were used in this protocol. ANOVA statistical analysis was utilized in determining significance with a Tukey-HSD post-hoc analysis. An alpha of 0.05 was used as the cutoff for significance. SAS JMP (SAS JMP Pro Version 13, SAS Institute Inc., Cary, NC, USA) was used for statistical software. The standard error of the mean was used in graphing error bars. The one-way ANOVA statistical analysis was performed via Tukey HSD post hoc analysis (p=0.05). Samples that do not share a letter are significantly different. Samples that share a common letter are not significantly different.

Cellular ROS

Cellular ROS detection assay was carried out with modification to an existing protocol[38]. The 2,7-dichlorofluorescin diacetate (DCFDA) cellular ROS detection assay kit was ordered from Abcam (ab113851). Briefly, yeast strain BY4741 was grown to stationary-phase in YPD supplemented with DCFDA without light at 30°C. Cultures were centrifuged and washed in phosphate-buffered solution before being resuspended YM+HULM to a final OD_{600} of 0.7. Yeast were treated for 90 minutes, CMC-Cu at 157 μM and $CuSO_4$ at 400 μM, and controls, H_2O_2 at 489 μM, in a 96 well black bottom microplate from Greiner Bio-One for end-point fluorescence measurement at Ex/Em = 485/535 nm on a SpectraMax Gemini XPS Fluorescence Microplate Reader from Molecular

Devices. Five biological replicates were used in this protocol. ANOVA statistical analysis was utilized in determining significance with a Tukey-HSD post-hoc analysis. An alpha of 0.05 was used as the cutoff for significance. SAS JMP (SAS JMP Pro Version 13, SAS Institute Inc., Cary, NC, USA) was used for statistical software. The standard error of the mean was used in graphing error bars.

Lipid Peroxidation

Lipid peroxidation was colorimetrically measured by assessing the major byproduct of lipid peroxidation, malondialdehyde, in a Thiobartic Acid Reactive Substances assay (TBARS). The OxiSelect™ TBARS assay kit (STA-330) was obtained from CellBioLabs, Inc, San Diego, CA, USA. Yeast strain YJM339 was grown in triplicate until log phase in YM at 30°C. Yeast cells were harvested at a final OD_{600} of 0.7, treated with 400 μM CuSO4, 157 μM CMC-Cu, or 498 μM H_2O_2 for 90 minutes. A kit-supplied SDS lysis solution (Part No. 233003) was incubated within both the samples and the malondialdehyde (MDA) standards (Part No. 233001) at 1:1 ratio totaling 200 μl for five minutes at 23°C. 250 μl of thiobartic acid reagent (5.2 mg mL^{-1} at pH 3.5) (Part Nos. 233002 & 233004) was added to each sample and incubated at 95°C for 50 minutes. Samples were cooled in an ice bath for five minutes before 15 minutes of centrifugation at 3,000 g. The supernatant was harvested and aliquoted for duplicate technical spectrophotometric measurement in a TECAN Infinite 200 pro microplate reader at 532nm absorbance. TBARS levels were determined from an MDA equivalence standard curve ranging from 0 to 125μM. ANOVA statistical analysis was performed with Tukey-HSD post-hoc analysis. An alpha of 0.05 was used as the cutoff for significance. SAS JMP (SAS JMP Pro, Version 13, SAS Institute Inc., Cary, NC, USA) was used for the construction of the whisker-box plots.

Electron Microscopy

Yeast strain BY4741 was grown in YM+HULM until log-phase at 30°C. Cells were treated with CMC-Cu at 400 μM for 90 minutes before 6 ml were harvested by centrifugation for 4 minutes at 3,000 g. The supernatant was pipetted off and the cells were resuspended in 500 μl of paraformaldehyde (14%) for one hour at room temperature. Fixed cells were washed once and resuspended in 0.1 M KPO4/1.2 M sorbitol buffer for storage at 4°C. Within 72 hours in the WVU Electron Microscopy Facility, the cells were fixed with 2.5% glutaraldehyde for one hour before washing thrice with PBS for 15 min each. Samples were then aliquoted into Eppendorf tubes for either SEM or TEM processing and imaging.

The cells were dehydrated stepwise by 15 min ethanol baths starting at 30% and increasing to 50%, 70%, 90%, and finally, 100%. The 100% ethanol bath was repeated three times. Yeast cells were pelleted, and the supernatant was discarded after each ethanol addition. Samples were submerged in hexamethyldisilazane to dry the cells for 15 minutes before allowing the cells to air-dry overnight in a fume hood with the caps of the Eppendorf tubes slightly open. Samples were adhered to pins by carbon tape and sputtered with gold and pallidum (60:40) for 150 seconds at 18kV with rotation. A Denton Desk V Sputter and Carbon Coater were used in sputtering samples. Images were captured on a Hitachi S-4700 Scanning Electron Microscope.

DNA Damage

Damage to DNA and chromosomes was assessed by pulse-field gel electrophoresis (PFGE). Yeast strain BY4741 was grown to log phase in YM+HULM media at 30°C. Cells were treated with

H_2O_2 at 489 μM or CMC-Cu 400 μM up to 90 minutes. One OD_{600nm} unit of yeast cells was harvested by centrifugation in conical tubes at time points of 5 min, 15 min, 30 min, 60 min, and 90 min. The sample supernatant was removed and frozen in liquid nitrogen for storage at -80°C, sample processing occurred within 24 hours. Cells and zymolase enzymes at a final concentration of 0.05 μg/ml were mixed 1:1 with 2% low melting agarose gel diluted in 0.5x TBE to obtain 1 OD unit per plug. Plugs were made in a Bio-Rad disposable plug mold via heat block set to 50°C with a cut off pipette tip to facilitate the agarose mixing. The solidification of agarose plugs occurred for 15 min at 4°C. To digest the cell wall, 1 ml of plugs were placed in 5 ml of M/15 PBS supplemented with zymolase and incubated for 1 hour at 37°C without agitation. Plugs were washed with a wash buffer (20nM Tris, 50mM EDTA, pH 8). The protein was digested by adding a proteinase K buffer (30mM Tris, 50mM EDTA, 1% SDS, 0.125μg/ml proteinase K, pH 8) and incubating at 50°C overnight. Plugs were washed four times for 1 hour each at 23°C. Plugs were trimmed to ¾ original size, positioned onto the comb ends and adhered with one droplet of low melting agarose. A 1.5% PFGE gel was made using 0.5x TBE and Bio-Rad PFGE agarose by casting into a mold with the comb in position. After the gel solidified, the comb was removed, and the gel was placed into a Bio-Rad CHEF DR II system filled with 0.5x TBE equipped with a water cooler. Electrophoresis of the experimental gel occurred for 24 hours at 14°C with a switch time of 60-120 seconds and set to 6v/cm. The gel was removed, stained in a 0.125 μg/ml ethidium bromide bath for 10 minutes, and destained with distilled water for one hour before imaging at 254nm. Pictures were manipulated in Microsoft PowerPoint solely to straighten running lanes for added clarity.

Exploration of Lipidome

Lipid metabolites were assessed in *S. cerevisiae* YJM789, grown in YM to exponential phase (OD 0.4 – 0.6), and then treated or not for 90 minutes. Six independent biological replicates were performed. Five optical units of cells were harvested, washed with MQ (milliQ) water, and flash-frozen in liquid nitrogen for storage at -80°C until extraction within 24 hours. Lipid and polar metabolites were extracted with 6 ml of a 1:2:0.8 mixture of chloroform: MeOH: H2O, following a modified version of a published protocol[39,40]. Glassware was used to avoid polymer contamination. Extraction occurred in 15 mL Kimble™ Kontes™ KIMAX™ reusable High Strength Centrifuge Tubes from Fisher Scientific. HPLC-grade chloroform and methanol were from Sigma-Aldrich. Six replicates of 3ml each were harvested for their lipid phase and dried under nitrogen gas. The lipid phases were re-suspended in 500 μL 1:1 chloroform: MeOH and these extracts were stored at -20°C until analysis within 48 hours.

Lipid extracts were analyzed by direct injection using a Thermo Fisher Scientific QExactive, with an ESI (electrospray ionization), using positive and negative modes. For lipid compounds in positive mode, the injection speed was 10 μL/min, the scan range: 150.0 – 2,000.0 m/z, no fragmentation, 140,000 resolution, 1 microscan, AGC target 5 x 10^5, maximum injection time of 100, sheath gas flow rate of 15, aux gas flow rate of 11, no sweeping gas flow, spray voltage of 3.50 kV, capillary temperature of 300°C, S-lens RF level: 25.0. These same parameters were kept for lipid compounds in negative mode except for a spray voltage of 3.20 kV. For each sample, a total of 50 scans were obtained and averaged with Thermo Scientific Xcalibur 2.1 SP1. Averaged spectra in the positive and negative mode were processed with xcms 3.2.0[41]. Peaks were identified within each spectrum using the mass spec wavelet method from the MassSpecWavelet 1.46.0 R package[42]. Peaks were grouped via the Mzclust method, followed by group ChromPeaks. All

features were plotted and visually inspected. Intensity values of each sample feature were obtained via the featureValue method using the integrated signal area for each representative peak per sample. Feature intensity and feature definition tables were saved as CSV files. Features were identified via MetaboSearch 1.2[43]. The query ID list was comprised of the average mz values for each feature in positive or negative mode with 5 ppm of error and was searched against the four databases available online in the program: Human Metabolome Database (HMDB)[44], Metlin[45], Madison Metabolomics Consortium Database (MMCD)[46] and LipidMaps[47]. Identifications were manually cross-referenced with Yeast Metabolome Database (YMDB)[48] and PubChem[49]. Feature intensity tables were composed of only identified features from positive and negative modes with at least five biological replicates. MetaboAnalyst[50] was used for statistical analysis, data normalization to the intensity of all features, and generation of the graphical figures. The experiment was repeated twice with consistent results.

Results and Discussion

Metal Homeostasis

To explore compromised metal homeostasis induced by CMC-Cu exposure, the intracellular metal concentrations were quantified. Experimentally, the Zrt1 protein levels in copper resistant yeast S288c increases 2-fold in response to copper perturbation, suggesting some responsive role for the Zrt transporters[28]. Cellular copper and zinc levels were analyzed via Inductively Coupled Plasma – Optical Emission Spectroscopy (ICP-OES) after exposure to 400 µM $CuSO_4$ or 157 µM CMC-Cu which results in nearly equal growth inhibition of the copper sensitive strain[28]. During normal growth of the sensitive clinical isolate YJM789 in YM, ICP-OES analysis measured 0.043 mg mL^{-1} Cu, standard error (SE) 0.011 (Figure 1A and Figure S1). The resistant lab isolate, BY4741 is derived from the S288c and contains additional auxotrophic markers. The copper content in BY4741 under normal growth conditions was undetectable (Figure 1B). Unsupplemented YM media supplies 0.16 nM Cu in the growth medium. After $CuSO_4$ addition, copper levels increased for each strain. The level of copper in YM is not optimal for BY4741 because the addition of 50 µM $CuSO_4$ increases growth[28], suggesting that BY4741 is copper deficient in standard growth media. With $CuSO_4$, copper levels rose but to differing degrees. YJM789 had 1.223 mg mL^{-1} Cu, SE

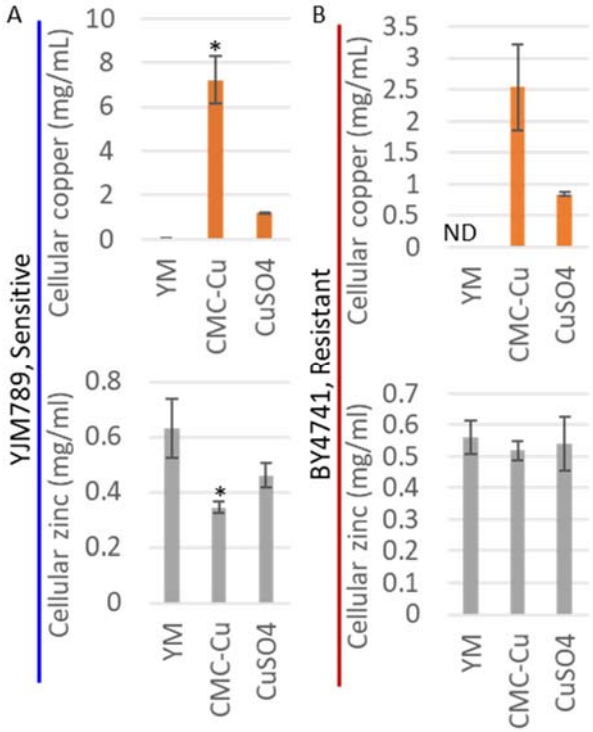

Figure 1 **Copper and Zinc Metal Homeostasis Measured by Inductively Coupled Plasma – Optical Emissions Spectroscopy During CMC-Cu Toxicity.** Sensitive strain YJM789 (A) and resistant strain BY4741 (B) were harvested after 90-minute treatments with CMC-Cu or $CuSO_4$. (A) YJM789 has a significant increase in cell-associated copper with CMC-Cu treatment and a decrease in cellular zinc. (B) BY4741 showed an increase of cellular copper with CMC-Cu treatment, no change to zinc concentrations. Statistical analysis performed via one-way ANOVA with a post hoc Tukey HSD analysis (p=0.05). ND= Not detected.

0.011 and BY4741 had 0.837 mg mL^{-1} Cu, SE 0.029. Copper levels increased in the resistant strain, BY4741, to 2.541 mg mL^{-1} Cu after CMC-Cu treatment. Tukey-Kramer honest significance difference (Tukey-HSD) post-hoc statistical analysis showed no statistical difference between copper levels of either CMC-Cu or $CuSO_4$ treated cells of either strain with one exception (Table 1). The sensitive strain, YJM789, increased its copper concentration to 7.230 mg mL^{-1} Cu, SE 1.086 after treatment with CMC-Cu. Intracellular copper concentrations were only significantly increased when YJM789 was exposed to CMC-Cu ($p<0.001$).

Table 1. Connecting Letters Statistical Report for Copper and Zinc Levels by Strain and Treatment. Statistical analysis performed via one-way ANOVA with a post hoc Tukey HSD analysis (p=0.05). Samples that share a common letter are not significantly different. Samples that do not share a letter are significantly different.

Zn		
	YJM789	**BY4741**
YM	**A**	**A**
CMC-Cu	**B**	**A,B**
CuSO4	**A,B**	**A,B**

Cu		
	YJM789	**BY4741**
YM	**C**	**A,B,C**
CMC-Cu	**A**	**A,B**
CuSO4	**B**	**B**

Zinc is a divalent transition metal that binds to ligands less stably than copper according to the Irving-Williams series[20]. The concentration of cellular zinc significantly decreased from the YM baseline of 0.632 mg mL^{-1} zinc for yeast strain YJM789 in response to CMC-Cu treatment, resulting in a cellular concentration of 0.344 mg mL^{-1} Zn, SE 0.0449 ($p=0.028$). In response to CMC-Cu treatment, the sensitive strain, YJM789, increased levels of copper while decreased the levels of zinc. This evidence suggests that metal homeostasis of zinc and copper influences the toxicity of CMC-Cu. Zinc metallates 582 potential zinc-binding proteins contributing to the structure and function of approximately ~ 10% of the total yeast proteome[21]. *S. cerevisiae* yeast have a minimum zinc quota of $\sim 10^7$ atoms/cell[51], most of which is tightly controlled allowing a low level of labile zinc[52–54]. This labile zinc is maintained via intercellular storage in organelles, in the cytosol by dynamic metallothioneins that buffer redox activity, and in intracellular yeast vesicle compartments that resemble mammalian zincosomes[55–57]. The cellular zinc levels of the other conditions and strains were all statistically the same. After $CuSO_4$ treatment, YJM789 zinc levels decreased from 0.632 mg mL^{-1} to 0.46 mg mL^{-1}. BY4741, the copper resistant strain, in YM had 0.562 mg mL^{-1} of zinc. CMC-Cu treatment did not significantly change the levels of zinc nor did $CuSO_4$ in the copper resistant strain. The levels of zinc in YJM789 treated with CMC-Cu decreased to nearly half compared to the yeast grown in YM. The findings presented here align with literature reports implicating a role for zinc in copper nanoparticle toxicity[28]. The compromised metal homeostasis observed in YJM789 is likely involved in this strain sensitivity towards copper. One possible explanation of the relationship seen between falling Zn and increasing Cu levels involves the stability of transition-metal complexes as described by the Irving-Williams series. In this trend, divalent transition metals create an increasingly stable complex

resulting with copper as the most favored. The ligands selection bias is as follows: $Mn^{2+} < Fe^{2+} < Co^{2+} < Ni^{2+} < Cu^{2+} > Zn^{2+}$[20] and this is related to size and charge of the metals. As seen in other reports, one way this unbalance may propagate is through ionic mimicry, where zinc or other transporters select copper instead of zinc[58]. This chemical tendency between metal atoms not only is a factor of CMC-Cu toxicity but also is a factor in antimicrobial metal toxicity. The mechanism by which the different forms of Cu affect Zn levels are unclear, and this is likely involved with enhanced delivery of Cu to the cytoplasm in the YJM789 strain[28]. The high-affinity zinc transporter, Zrt1, has been previously shown attribute to the Cu resistance in mutational analysis and QTL analysis found the low-affinity zinc transporter, Zrt2, that has five amino acid polymorphisms between the two yeast strains that contributes to Cu sensitivity of YJM789[28]. Studies investigating copper uptake and kinetics found that the kinetic uptake for copper in *S. cerevisiae* is $V_{max} = 0.21$ nmol Cu min^{-1} (mg protein)$^{-1}$ with a $K_m = 4.4\mu M$[59] and that accumulation of Cu decreases in the presence of Zn^{2+}[60]. The zinc transporters of YJM789 are likely participating in an ionic/molecular mimicry mechanism importing CMC-Cu. The spatial concentration of CuNPs from CMC-Cu on the cellular surface may influence the difference in ionic mimicry between the two forms of copper in this research.

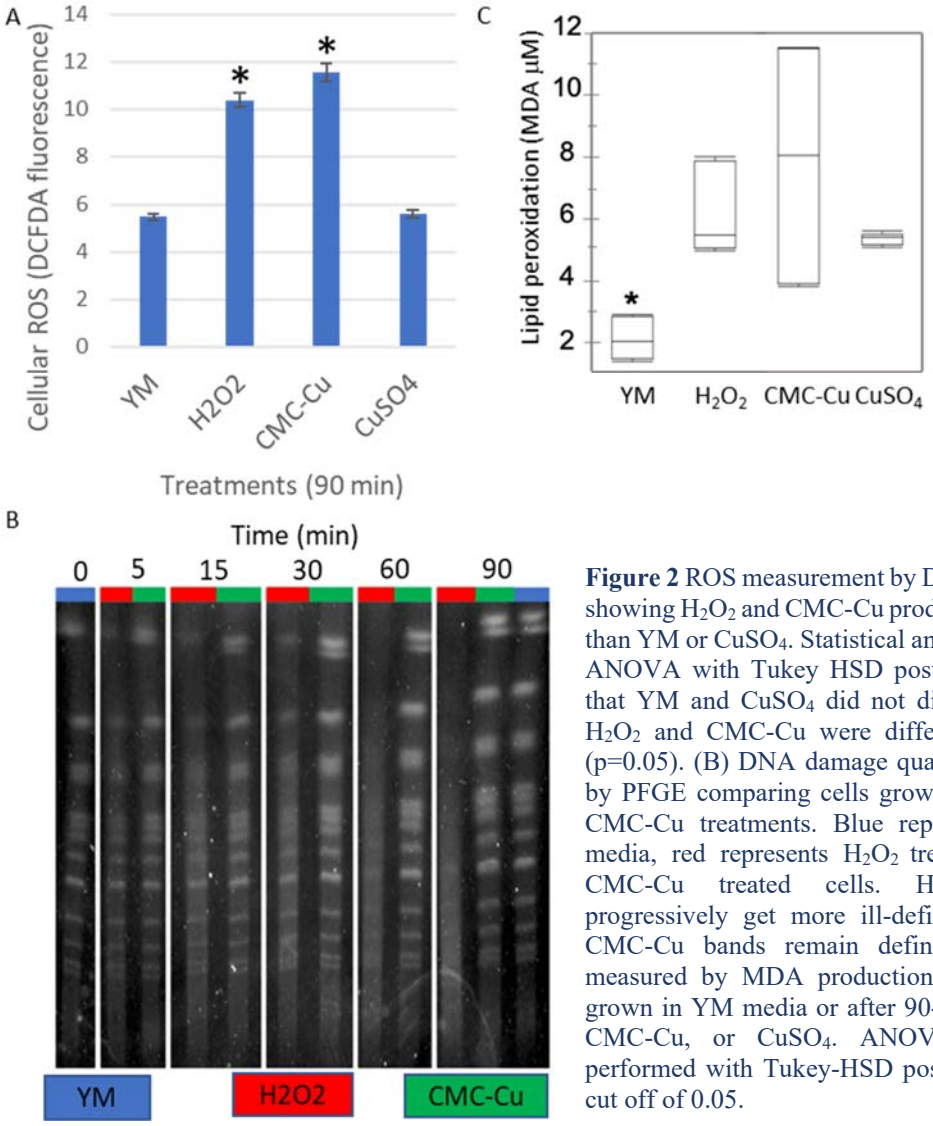

Figure 2 ROS measurement by DCFDA fluorescence intensity showing H_2O_2 and CMC-Cu producing higher amounts of ROS than YM or $CuSO_4$. Statistical analysis performed via one-way ANOVA with Tukey HSD post-hoc analysis that suggested that YM and $CuSO_4$ did not differ significantly while both H_2O_2 and CMC-Cu were different from all other samples ($p=0.05$). (B) DNA damage qualitative assessment over time by PFGE comparing cells grown in YM media to H_2O_2 and CMC-Cu treatments. Blue represents cells grown in YM media, red represents H_2O_2 treated cells, green represents CMC-Cu treated cells. H_2O_2 Chromosomal bands progressively get more ill-defined after 15 minutes while CMC-Cu bands remain defined. (C) Lipid peroxidation measured by MDA production via TBARS assay of cells grown in YM media or after 90-minute treatment with H_2O_2, CMC-Cu, or $CuSO_4$. ANOVA statistical analysis was performed with Tukey-HSD post-hoc analysis and a p-value cut off of 0.05.

Intracellular Reactive Oxygen Species

As a redox-active metal, copper is well-known to proliferate ROS and this study sought to investigate ROS as a toxicological mechanism of CMC-Cu exposure. Endogenous ROS is produced through aerobic respiration

giving rise to incompletely reduced forms of molecular oxygen (O_2) which yield hydrogen peroxide (H_2O_2) and hydroxyl radical ($^{\cdot-}O_2$). In the presence of a redox-active metal, Fenton reaction driven autooxidation occurs. To measure intracellular ROS, a fluorometric assay utilizing 2,7-dichlorofluorescin diacetate (DCFDA) was measured at the standard 90 min treatment (Figure 2A) and over time (Figure S2) which showed the differences in ROS between treatment groups as they biologically interacted with the perturbations. CMC-Cu treatments of 157 μM produced high amounts of ROS measured at 11.35 fluorescence (FC), SE 0.26 (Figure 2A); nearly double the endogenous ROS levels in YM. Hydrogen peroxide (H_2O_2) treatments at 489 μM produced similar levels of intracellular ROS levels of 10.38 FC, SE 0.26. Although soluble and nano-copper treatments were determined to inhibit growth at similar levels[28], the 400 μM treatment of $CuSO_4$ did not produce significant enough levels of ROS via this DCFDA assay. The yeast used here, BY4741, tolerated 400 μM $CuSO_4$ well. It is likely that increased ROS detection would occur by exposing this yeast to increased levels of $CuSO_4$, which would increase the growth inhibition of this resistant strain. $CuSO_4$ treatments produced intracellular ROS levels of 5.62 FC, SE 0.26 which was similar to the level detected in untreated control cells. ROS was detected at 5.5 FC, SE 0.26 in untreated cells (YM). Post-hoc statistical analysis via Tukey-Kramer honest significance difference (Tukey-HSD) analysis defined three detection levels between the samples, a low-level ROS group of $CuSO_4$/ YM and two different high-level ROS groups composed of either H_2O_2 or CMC-Cu. Reduction potential is a key factor when determining the toxicity of antimicrobial metals. In bacteria, there have been at least three mechanisms suggested for the increased ROS produced via metal poisoning. They include catalyzing Fenton chemistry[61,62], disruption of iron ligands such as Fe-S clusters that release redox-active Fe[63,64], and thiol mediated reduction of metal species[62,65]. Importantly, the oxidation of cellular thiols occurs via Cu-S covalent bonding which leads to disulfide bonds in proteins, thus depleting critical antioxidants including glutathione, ultimately preventing cellular repair[2,66–68]. The glutathione tripeptide molecule contains thiol ligand groups in their cysteine amino acid. This sulfur-containing molecule reduces copper by donating an electron to copper, which results in oxidation of the thiol group inducing a disulfide bond between cysteines of two glutathione molecules. While in yeast, $CuSO_4$ toxicity is recused by both glutathione and precursor N-acetylcysteine, but CMC-Cu toxicity is only rescued by glutathione[28]. Several adaptations and resistance mechanisms in *S. cerevisiae* are known, of which the intracellular sequestration of Cu and the yeast strain resistance is largely predicted by the variation in copy number metallothionein Cup1. This copy number variation and resistance is seen in the type and sequence strain, S288c[69,70], from which the BY4741 strain used here is derived. This evidence, together with the findings on intracellular ROS suggesting that the reduction potential of CMC-Cu, contributes to its unique nanotoxicity.

Genotoxicity

In an approach to identify the primary process and kinetics of CMC-Cu induced ROS damage to the yeast cells, the possibility of DNA damage was explored via a timed pulse-field gel electrophoresis (PFGE). As DNA is damaged, the accumulation of breaks causes the distinct chromosomal bands to be lost. The more ambiguous the chromosomal bands are in the PFGE, the more DNA damage has occurred. DNA damage by ROS has been well documented and implicated in mutagenesis and carcinogenesis[71], but there remains some discussion about its role in the primary damaging process. Hydrogen peroxide and the superoxide anion damage DNA by creation of the hydroxyl radical and singlet oxygen which are energetic enough to have a direct effect on DNA[72,73]. CMC-Cu at 157 μM caused little to no DNA damage over this study's typical 90-minute

treatment when measured qualitatively by inspecting the chromosomal band integrity in the PFGE gel (Figure 2B). The chromosomal band integrity, band intensity, and background smearing of CMC-Cu treated cells with those of the YM control were very similar in pattern. When treated with 489 μM of H_20_2 over time, a shift in the chromosomal band integrity was seen staring at the 15-minute mark and progressing until the 90-minute mark where all chromosomal band integrity was lost to DNA fragmentation represented as smearing across the gel. Hydrogen peroxide[74] and copper at moderately toxic concentrations induce apoptosis in *S. cerevisiae*[75]. DNA fragmentation, phosphatidylserine externalization, and chromatin condensation are typical markers of yeast apoptosis[76]. Highly toxic levels of Cu induce necrosis from which the mitochondria has been implicated to play a role[75]. With these findings in sight, the hypothesis that CMC-Cu treatment under these conditions lacked DNA fragmentation, but induced lipid damage to the cellular membrane damage was formed.

Lipid Peroxidation

Aside from DNA, another target of cellular damage is the lipid membrane of the cell, and a compromised cellular membrane is a major action of antimicrobial copper. This investigation aimed to determine if lipid peroxidation was the primary process of CMC-Cu induced ROS damage to *S. cerevisiae*. ROS-induced lipid peroxidation[77–79] and *S. cerevisiae*'s cellular fatty acid composition-dependent susceptibility to copper[12] was considered in forming this hypothesis. During lipid peroxidation, byproducts are formed of which malondialdehyde (MDA) is a convenient biomarker for lipid peroxidation[80,81]. Thiobarbituric acid (TBA) reacts with MDA forming a deeply colored chromogen fluorescently red adduct TBA-MDA[82]. By utilizing this reaction, lipid peroxidation was investigated by measuring the MDA-TBA adduct in a fluorescence assay known as a thiobarbituric acid reactive substances assay (TBARS). Dunnett's post-hoc statistical analysis found that the CMC-Cu, $CuSO_4$, and H_2O_2 treatments all induced lipid peroxidation compared to the YM control media (Figure 2C). CMC-Cu treated cells analyzed via the TBARS assay produced the greatest fluorescence measuring at 8.03μM MDA and within the biological replicates there was a wide-range. During this experiment a relatively large amount of variation between the CMC-Cu exposures was found. This is likely related to particle size distribution and degree of agglomeration of the particles. Levels of lipid peroxidation caused by hydrogen peroxide and copper sulfate treated cells were very similar, measuring 5.60 μM and 5.47 μM MDA, respectively. These findings supported previous reports of copper's toxic interaction with cell membranes[13,36]. The control sample in YM media measured 2.12 μM MDA. Unsaturated fatty acids are a major target of ROS that results in a cyclic reaction[83,84] generating lipid radicals and toxic lipid hydroperoxides[73,85]. Hydroperoxides are unstable in the presence of metals and they are the primary product of lipid peroxidation. They attach to lipids such as free fatty acids, triacylglycerols, sterols, and phospholipids. *In vivo* decomposition of these compounds occurs via the reduction, in part enzymatically, by glutathione peroxidase typically using glutathione as a reductant[82]. This process ultimately leads to loss of membrane integrity and generation of aldehydes that can cause distant and localized lipid peroxidation[86,87]. The evidence that CMC-Cu and $CuSO_4$initiated lipid peroxidation supports the hypothesis that the primary process of CMC-Cu induced ROS damage to *S. cerevisiae* is lipid peroxidation.

Lipid Profiling

This study's results indicate that CMC-Cu induced ROS facilitated lipid peroxidation, but to further define the details of CMC-Cu nanotoxicity an untargeted exploratory metabolomics

assessment was employed. By utilizing a gas chromatography with electron spray ionization mass-spectroscopy (GC-ESI-MS) methodology the lipidomics aspect proved most interesting. Lipid extracts analyzed in the positive and negative modes of ESI-MS provided 610 potential features that were chiseled down to yield 105 tentative structure confidence level annotated compounds (Table S1). These were used as variables in the statistical analysis performed in MetaboAnalyst 4.0. A partial least squared discriminant analysis (PLS-DA) technique was adequate in discriminating samples into their treatment groups of YM, CMC-Cu, $CuSO_4$, and CMC. A loadings matrix was made for the PLS-DA (Table S2). A PCA score plot, loading plot, and statistical ANOVA analysis was produced (Figure S3), but the PCA did not provide as good of separation as the PLS-DA. Using three components, a clear separation between all of the treatment groups was found. By using 2 components, 1 and 2, the PLS-DA had an overlap of the YM control and CMC-Cu treatment (Figure 3A). With components 1 and 3, the PLS-DA had an overlap of

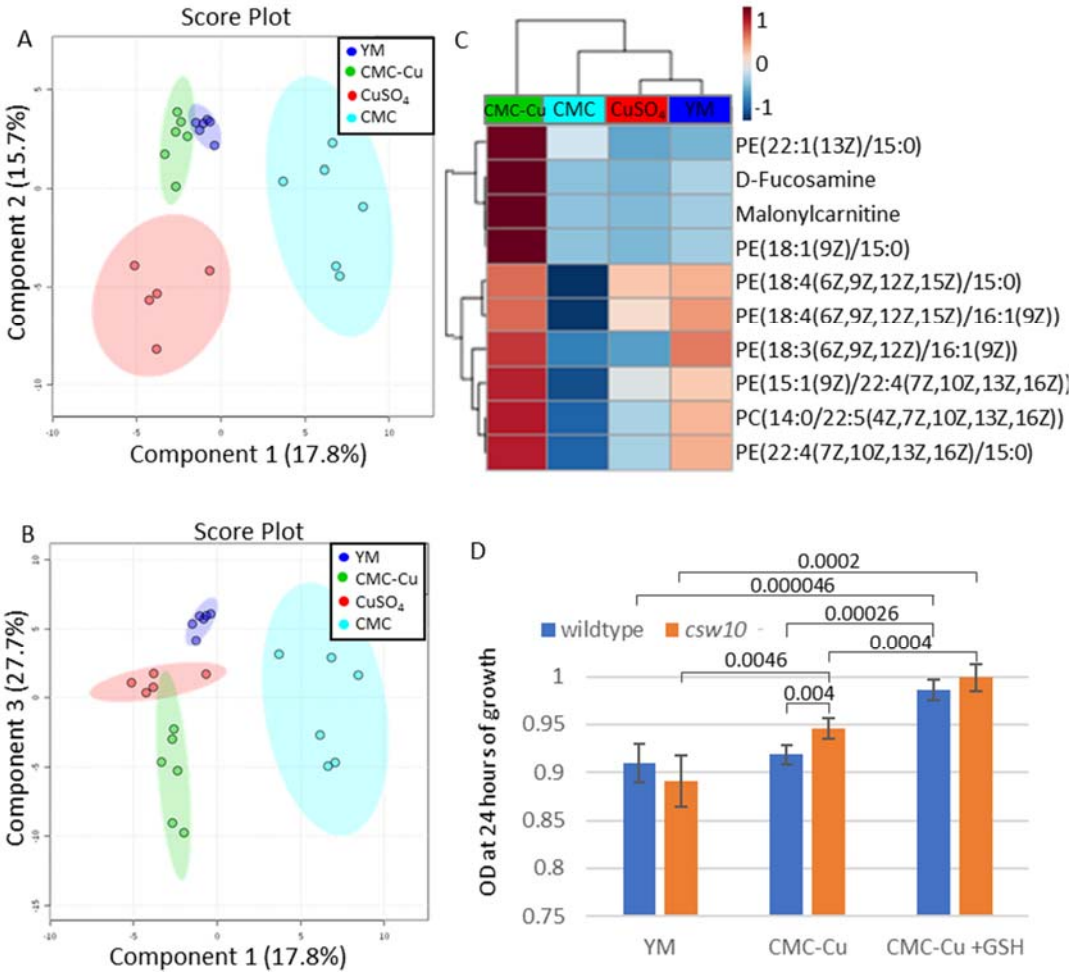

Figure 3 **Lipid Metabolic Profiling in Response to CMC-Cu Treatment.** (A) Partial least squares discriminant analysis (PLS-DA) showing component 1 and component 2 separated all treatments but YM and CMC-Cu. (B) PLS-DA showing component 1 and component 3 separated all treatments but YM and CMC-Cu, as well as CMC-Cu and $CuSO_4$. Taken together, components 1, 2, and 3 provide a 3-dimensional separation of all treatments based on their lipid profiles. (C) Heatmap of the top 10 metabolites used in profiling yeast treatment groups. Samples are divided into columns, compounds are divided by rows, and the color is indicative of relative abundance. Which was calculated via MetaboAnalyst hierarchical heatmap clustering analysis (clustering distance using euclidean, and clustering algorithm using ward D). (D) Quantitative growth assays of BY4742 (wildtype) and *scw10* isogenic mutant in YM, YM+CMC-Cu, and YM+CMC-Cu with glutathione (GSH). The average of four biological replicates were graphed with standard error after 24 hours of growth.

CMC-Cu and $CuSO_4$ treatments (Figure 3B). A permutation test was administered that showed the supervised method did not overfit the data, enabling interpretation of the results, $p< 0.001$. This result is suggestive of the similarity between soluble copper toxicity but also supportive of the unique nature of the CMC-Cu nanotoxicity. Component 1 explained 17.8% of the variance, component 2 explained 15.7%, and component 3 explained 27.7% of the variance between samples. The heatmap (Figure 3C) of the top 10 compounds averaged per treatment groups showed the cellular membrane phospholipids phosphatidylethanolamine (PE) and phosphatidylcholine (PC) increased in relative abundance for CMC-Cu treatments. A whole lipidome heatmap was also generated (Figure S4). *In vitro* studies have shown that copper ions interact with synthetic membrane models in an ordered fashion first with PC, then PE based on the structure of the membrane prevalent phospholipids[13]. Moreover, a study on heavy metals interaction with the mycelia lipids of *P. marquandii* utilized high performance liquid chromatography – tandem mass spectroscopy (HPLC-MS/MS) to find the ratio of PE:PC changed, increasing the PC content upon exposure to copper ions[88]. PC and PE composition responded to CMC-Cu and $CuSO_4$ exposure, albeit in opposing fashion. Unexpectedly, CMC had a depleting effect on lipid composition. PC and PE are the chief membrane lipid components from which their composition influences physico-chemical properties altering basic biological function in yeast such as cell growth, budding, membrane trafficking, and other formations[89–91].

The biosynthesis of fatty acids/ acyl chains starts with the conversion of acetyl-CoA into malonyl-CoA from which the acetyl chain develops mainly C16:0 and C18:0 before desaturation in the endoplasmic reticulum (ER) of *S. cerevisiae*[92]. This acyl-CoA pool can be then converted into bulk phospholipids through various pathways involving the ER and mitochondria[89]. The Kennedy pathway allows PE and PC formation from acyl-CoA and triacylglycerols (TG) pools. This study found that CMC-Cu treated cells depleted TG reserves (Figure S4) and increased important PE and PC levels (Figure 3), suggesting a disruption in lipid homeostasis. TGs stored in lipid droplets protect lipid homeostasis by balancing fatty acid saturation[93] and serving as a base for phospholipid metabolism[94]. When needed, TGs are hydrolyzed to provide building blocks for membrane lipid synthesis, delivering a quick response to changing environmental conditions[95]. TG can be converted to PC and PE through the Kennedy pathway[89,95]. These results support the hypothesis that CMC-Cu treated cells are depleted of their protective TG content through an increase in PC and PE membrane production.

Interestingly, in CMC-Cu treated yeast relatively high malonylcarnitine levels were found, a metabolite involved with the transportation of long-chain fatty acids into the mitochondria (Figure 3C). Increased levels of malonylcarnitine are indicative of fatty acid oxidation disruption and mitochondrial respiratory chain failure[96–100]. Cellular copper is distributed throughout the entire cell and a pool of bioavailable copper is also present within the mitochondria[101], enabling mitochondrial metallation reactions. Formation of the Cu centers bound within cytochrome c oxidase (CcO) occurs in the mitochondrial inner membrane space (IMS) during which two copper-binding subunits of CcO become metallated[102]. The detection of relatively high levels of malonylcarnitine further suggests that lipid damage is a primary target of the yeast cell damage, as this metabolite is indictive of fatty chain transportation disruption. Additionally, the amino-sugar fucosamine also increased in relative abundance during CMC-Cu treatment. Other amino-sugars such as fructosamine have been shown to complex with redox-active metals, chelating copper, iron, and nickel metals displaying some antioxidant aspects[103–105], although the research on

fucosamine is still in preliminary stages. Primary metabolites were also extracted and analyzed by GC-MS techniques but changes in the metabolism could not be used in a discriminating analysis without overfitting the data (data not shown). Together this lipid profiling and TBARS assay support lipid damage as a primary target of CMC-Cu induced nanotoxicity.

To assess how perturbations in lipid and cell wall metabolism could affect cell growth, quantitative growth of yeast containing knockouts of several candidate genes was measured. From the proteomics measurements, proteins that had levels change more than two-fold in the presence of $CuSO_4$ were selected[28]. We selected candidates that had known roles in oxidative stress, lipid metabolism, and cell wall synthesis. Sod2 is the mitochondrial superoxygen dismutase [106]. Ach1, a CoA transferase and hydrolase, is expressed in the mitochondria when grown on nonfermentable carbon sources[107]. Opi3 synthesizes phosphatidylcholine[108]. Mho1 is repressed by Opi1 when inosine and choline is present and is synthetically lethal with *PLC1* deletion which encodes a phospholipase C[109]. Gpx2, a phospholipid hydroperoxide glutathione peroxide, functions during oxidative stress to neutralize hydroperoxides[110] , Cts1, an chitinase that aids in separation of cell walls after mitosis[111], is also regulated by Ace2, a copper responsive transcription factor[112]. Scw10 is localized to the cell wall and resembles glucanases[113]. Each knockout strain was grown in YM+HULK to log phase and then diluted into media containing YM, YM with CMC-Cu, and CMC-Cu with glutathione and then monitored for 24 hours (Figure 3D). In the BY4742 background, yeast growth was not slowed at 24 hours. The addition of CMC-Cu did not change the growth. However, the addition of glutathione allowed yeast to grow to a higher density, suggesting that even under standard growth conditions yeast were under oxidative stress. Of all the mutants tested only the *scw10* mutant showed increased growth when CMC-Cu was added. The standard yeast media does not provide optimal levels of copper for growth of yeast from the BY background[28]. The loss of Scw10 protein from the cell wall may alter the association of the CMC-Cu with the cell wall. In YJM789 yeast, Scw10 increases 1.5 log2fold when treated with CuSO4 while the copper resistant strain Scw10 only increased 0.78 log2fold. The six other mutants in lipid and redox metabolism lack of a growth phenotype could be attributed to the robustness of overlapping pathways to response to stress.

Cell Surface Imaging

As the major phospholipid bilayer components PC and PE change in response to CMC-Cu exposure, the focus shifted to imaging the cellular damage and surface morphology in high-resolution detail by employing scanning electron microscopy (SEM). With the use of SEM, cell surfaces were visualized prior to and post-CMC-Cu treatment. Deformities in the cell surface resembled large invaginations post CMC-Cu exposure, as compared to the round and smooth cells grown in YM media (Figure 4). Log-phase cells grown in YM media were circular and oval in appearance (Figure 4A). The log phase cells were grown in YM with 157 μM CMC-Cu had surface deformations that are distinguished by red arrows (Figure 4B). Two images were chosen to be representative of treated and untreated population differences at 5,000 x magnification displaying the cellular surfaces of approximately 100 cells. At a higher 10,000 x magnification, varying degrees of cell surface invaginations on both mother and daughter cells (Figure 4C) were found. Ethanol treatment has been shown to produce a similar abnormal cell surface phenotype in yeast when visualized by electron micrographs[114]. These major alterations to the cellular structure have previously been used as a marker in characterizing novel antimicrobial treatments[115,116]. The previous report on CMC-Cu's toxicity to *S. cerevisiae* provided evidence supporting endocytosis

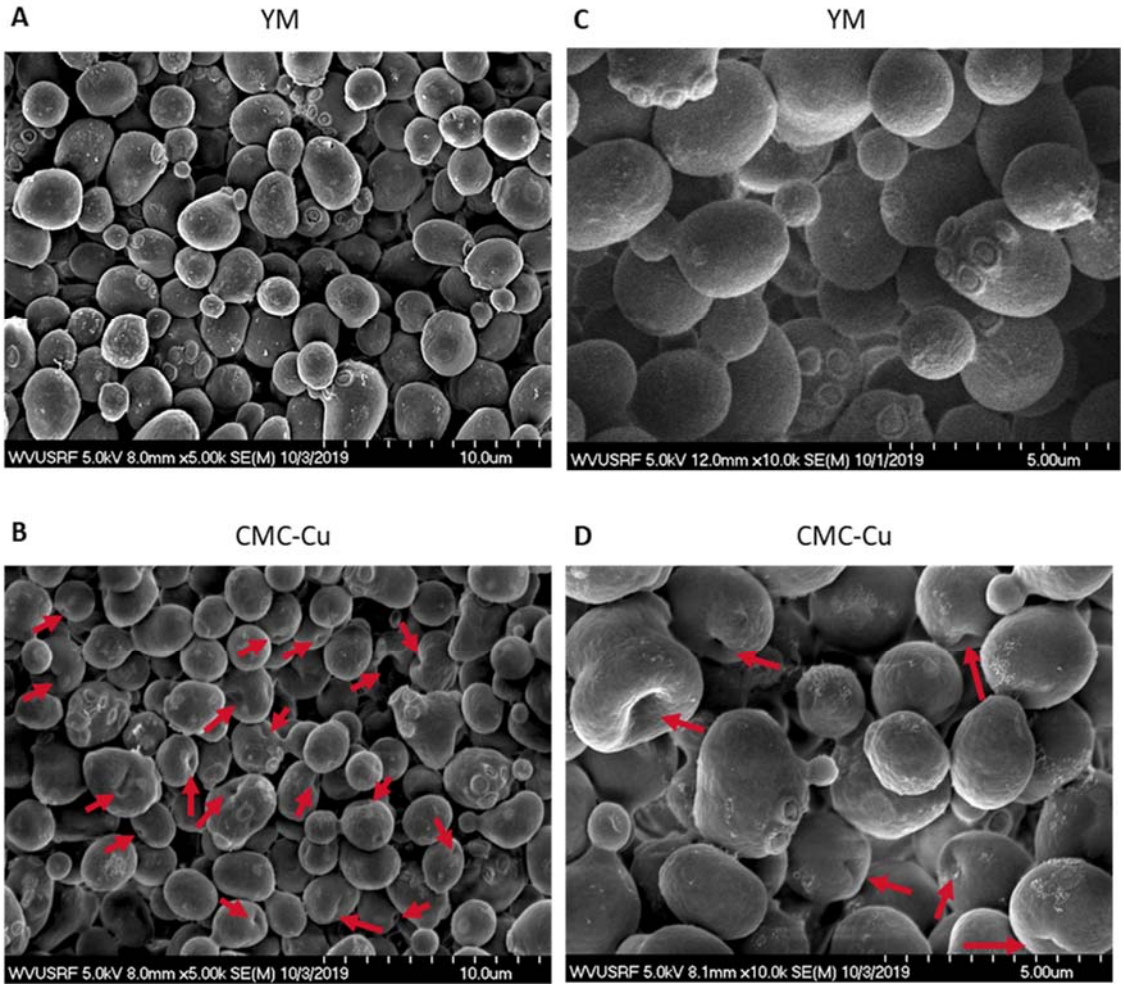

Figure 4 **Scanning Electron Micrographs of Yeast's Cellular Surface.** (A) Normal log-phase cells imaged at 5,000 x magnification with a smooth round or oblong surface grown in YM media without treatments. (B) Deformed log-phase cells imaged at 5,000 x magnification post CMC-Cu treatment. Surface invaginations shown with red arrows. (C) Normal log-phase cells imaged at 10,000 x magnification with a smooth round or oblong surface grown in YM media without treatments. (D) Close view of cellular deformities at 10,000 x magnification post CMC-Cu treatment.

of CMC-Cu by arrestins[28]. Here, the membrane curvature shown on the SEM micrographs appear not to be endocytosis vesicles because of the micrometer size of many of the invagination. Some of these invaginations alter the entire morphology of the yeast cell so much so that they resemble mammalian red blood cells. These abnormal morphologies of the cellular structure are indicative of cell surface damage. Previous reports show nanometer sized vesicles associated with actin patches via transmission electron microscopy (TEM)[117,118]. It is unlikely that these are a consequence of actin patches/ endocytosis, but the potential remains the that attempted endocytosis may be an antecedent to these invaginations. Direct membrane curvature by phospholipid modification[119] has supporting evidence from the lipid profiling and lipid peroxidation results shown here. Prior research concerning the location of CMC-Cu stained with Fluorescein isothiocyanate (FITC) suggested an association with the cellular surface for both CMC-Cu and CMC treatments[28]. Findings from the SEM images further support cell surface damage owing to membrane lipid peroxidation as the primary process by which CMC-Cu exerts its toxicity.

S. cerevisiae was chosen as a model system to investigate the nanotoxicity of the CMC-Cu exposures because of its genetic tractability, conserved genome, and exceptional wealth of experimental resources[120]. In *S. cerevisiae* arrestin knockouts, *aly1* and *aly2*, are viable when treated with CMC-Cu, unlike soluble copper[28]. This supports a role for endocytosis of CMC-Cu[28]. Arrestins have been suggested as a general model for transporter regulation[121,122]. Yeast α-arrestins are intracellular proteins that target specific plasma membrane proteins for the endocytic system[123] including metal transporter Smf1[122]. Once arrestins associate with plasma membrane proteins, ubiquitin-conjugating proteins are recruited. Ubiquitinated cargo is claimed for endocytosis and transfers into the vacuole for degradation via both clathrin-independent and clathrin-mediated endocytosis[124]. *S. cerevisiae* has a small ellipsoid, 60 - 30 nm in diameter, endocytic vesicle[125]. Endocytosis internalizes cargo from the plasma membrane and has a critical role in nutrient uptake, damaged protein turnover, membrane composition, and the response to extracellular signals. The organization and proper composition of the plasma membrane are maintained by endocytic downregulation of plasma membrane proteins during surface remodeling.

Conclusions

While performing an investigation into the nanotoxicological influence of CMC-Cu on metal homeostasis, ROS production, lipid interaction, cellular morphology, and genotoxicity several results were uncovered while using the *S. cerevisiae* model system. Metal homeostasis between zinc and copper becomes unbalanced, increasing Cu content and decreasing Zn content, in sensitive yeast strains upon treatment with CMC-Cu. Unbalanced Zn/ Cu metal homeostasis acts as a secondary nanotoxicological process during CMC-Cu exposure. This unbalance is possibly owing to the single nucleotide polymorphisms (SNPs) of *ZRT2* between genetically diverse yeast strains[28], mis-metallation, or ionic mimicry. Exposure to CMC-Cu produces ROS that did not indicate DNA damage but did suggest lipid peroxidation. Further exploration revealed that CMC-Cu altered the major membrane phospholipids, PC and PE, and depleted TG lipids that act to balance fatty acid saturation. This interaction between PC, PE, and TG suggest CMC-Cu has an influence on the Kennedy Pathway. These findings align with literature associating lipid damage with copper's antimicrobial mode of toxicity and Cu's interaction with PE and PC ,the major membrane phospholipid bilayer components[13,36,126]. The findings on CMC-Cu interaction with PC and PE adds to the limited body of research pertaining to coppers influence on biological lipids. Moreover, inspection of a detailed scanning electron micrograph showed an abnormal cellular morphology induced by CMC-Cu treatment. The visualized cellular surface disfigurement provides supporting evidence for surface membrane damage as the primary mechanism of action of CMC-Cu exposure in *S. cerevisiae*.

The previous study provided evidence that CMC-Cu physically interacts with the cellular surface and that α-arrestins Aly1 and Aly2 facilitate endocytosis of the copper nanoparticles into the cell[28]. An endocytosis mechanism likely attempts to partially or fully import CMC-Cu. Perhaps this endocytosis event disfigures the cellular morphology as an antecedent or consequence of CMC-Cu's physical interaction. Cumulatively, this evidence suggests CMC-Cu nanotoxicity occurs via localized damage primarily to the cellular membrane with secondary damages occurring via disruption of metal homeostasis and disruption of cellular functions likely in or near the vacuole and mitochondria. Thus far, the difference in antioxidant rescue suggests an exogenous

toxicological aspect[28], knockouts of arrestins rescue suggest association with an endocytosis event[28], high lipid peroxidation levels, high ROS levels, unbalanced Cu/ Zn homeostasis, and their unique influence on membrane lipids separates CMC-Cu from $CuSO_4$ There are also many overlaps in the toxicity and nanotoxicity of copper, such as the genetically diverse yeast strains' sensitivity to soluble copper is also mirrored by their sensitivity to CMC-Cu[28]. This is likely from the genetic and transcriptional regulation of metallothiones such as Cup1[28]. As nanotechnology evolves to synthesize advanced hybrid nanomaterials and their ubiquity throughout society increases, the demand for understanding biology's interaction with these materials will mature.

Figure Legends

Figure 1. Copper and Zinc Metal Homeostasis Measured by Inductively Coupled Plasma – Optical Emissions Spectroscopy During CMC-Cu Toxicity. Sensitive strain YJM789 (A) and resistant strain BY4741 (B) were harvested after 90-minute treatments with CMC-Cu or $CuSO_4$. (A) YJM789 has a significant increase in cell-associated copper with CMC-Cu treatment and a decrease in cellular zinc. (B) BY4741 showed an increase of cellular copper with CMC-Cu treatment, no change to zinc concentrations. Statistical analysis performed via one-way ANOVA with a post hoc Tukey HSD analysis ($p=0.05$). ND= Not detected.

Figure 2. Cellular Toxicity Profiles Including ROS Generation and Biomolecule Damage. (A) ROS measurement by DCFDA fluorescence intensity showing H_2O_2 and CMC-Cu producing higher amounts of ROS than YM or $CuSO_4$. Statistical analysis performed via one-way ANOVA with Tukey HSD post-hoc analysis that suggested that YM and $CuSO_4$ did not differ significantly while both H_2O_2 and CMC-Cu were different from all other samples ($p=0.05$). (B) DNA damage qualitative assessment over time by PFGE comparing cells grown in YM media to H_2O_2 and CMC-Cu treatments. Blue represents cells grown in YM media, red represents H_2O_2 treated cells, green represents CMC-Cu treated cells. H_2O_2 Chromosomal bands progressively get more ill-defined after 15 minutes while CMC-Cu bands remain defined. (C) Lipid peroxidation measured by MDA production via TBARS assay of cells grown in YM media or after 90-minute treatment with H_2O_2, CMC-Cu, or $CuSO_4$. ANOVA statistical analysis was performed with Tukey-HSD post-hoc analysis and a p-value cut off of 0.05.

Figure 3. Lipid Metabolic Profiling in Response to CMC-Cu Treatment. (A) Partial least squares discriminant analysis (PLS-DA) showing component 1 and component 2 separated all treatments but YM and CMC-Cu. (B) PLS-DA showing component 1 and component 3 separated all treatments but YM and CMC-Cu, as well as CMC-Cu and $CuSO_4$. Taken together, components 1, 2, and 3 provide a 3-dimensional separation of all treatments based on their lipid profiles. (C) Heatmap of the top 10 metabolites used in profiling yeast treatment groups. Samples are divided into columns, compounds are divided by rows, and the color is indicative of relative abundance. Which was calculated via MetaboAnalyst hierarchical heatmap clustering analysis (clustering distance using euclidean, and clustering algorithm using ward D). (D) Quantitative growth assays of BY4742 (wildtype) and *scw10* isogenic mutant in YM, YM+CMC-Cu, and YM+CMC-Cu with glutathione (GSH). The average of four biological replicates were graphed with standard error after 24 hours of growth.

Figure 4. Scanning Electron Micrographs of Yeast's Cellular Surface. (A) Normal log-phase cells imaged at 5,000 x magnification with a smooth round or oblong surface grown in YM media without treatments. (B) Deformed log-phase cells imaged at 5,000 x magnification post CMC-Cu treatment. Surface invaginations shown with red arrows. (C) Normal log-phase cells imaged at 10,000 x magnification with a smooth round or oblong surface grown in YM media without treatments. (D) Close view of cellular deformities at 10,000 x magnification post CMC-Cu treatment.

Figure S1. Copper Homeostasis During CMC-Cu Toxicity Represented in Treatment Groups. (A) Copper levels after normal log phase cell growth in YM. (B) Copper levels after CMC-Cu treatment. (C) Copper levels after $CuSO_4$ treatment. Red bars represent the resistant strain BY4741. Silver bars represent the sensitive strain YJM789.

Figure S2. Cellular ROS Generation Over Time. ROS measurement by DCFDA fluorescence intensity showing H_2O_2 and CMC-Cu producing higher amounts of ROS than YM or $CuSO_4$. Endpoint (90 min) statistical analysis performed via one-way ANOVA with Tukey HSD post-hoc analysis that suggested that YM and $CuSO_4$ did not differ significantly while both CMC-Cu and H_2O_2 were different from all other samples ($p=0.05$).

Figure S3. Lipidomic Statistics for CMC-Cu Treatment. (A) Unsupervised principal component analysis (PCA) of yeast grown in YM and treated with CMC-Cu, $CuSO_4$, or YM media showing incomplete separation of all treatments. (B) Loading plot for the PCA seen in part B. (C) Important compounds identified by One-way ANOVA with a Tukey HSD post-hoc analysis. The significance is presented on the y-axis with red dots indicating a significance greater than $p=0.05$ as indicated by the dashed line and insignificant dots in green. Of the compounds detected, select compounds of importance as identified in the heatmap analysis are labeled by name.

Figure S4. Whole Lipidome Heatmap for CMC-Cu Treatment. Color indicates the relative abundance on a Log2 fold change of the complete heatmap by each sample.

Table S1. Normalized Gas Chromatography Electrospray Ionization Mass Spectrometry Data. Column headers contain the ID compound and the rows are organized by the individual samples.

Table S2. Loading Matrix for PLS-DA Lipidomic Assay. Column headers contain each principal component and the rows are organized by the individual ID compounds.

Acknowledgments: MJW was supported by the Nation Science Foundation's Integrative Graduate Education and Research Traineeship: Research and Education in Nanotoxicology at West Virginia University (IGERT:REN@WVU) award number 1144676. We acknowledge Amaury Pupo Meriño for help with the GC-ESI/MS study and analysis, Marcela Redigolo for help using the electron microscope, Dr. Jonathan Cumming for help with the ICP-OES, Dr. Gloria Oporto for generously supplying the nanoparticles, Dr. Kang Mo Ku for help with the metabolomics studies, and The WVU Genomics Corps for use of their instruments.

The authors state no conflict of interest. Any opinions, findings, and conclusions or recommendations expressed in this material are those of the author(s) and do not necessarily reflect the views of the National Science Foundation.

References

1 J. Gabbay, G. Borkow, J. Mishal, E. Magen, R. Zatcoff and Y. Shemer-Avni, *J. Ind. Text.*, 2006, **35**, 323–335.

2 H. Palza, *Int. J. Mol. Sci.*, 2015, **16**, 2099–2116.

3 N. Cioffi, L. Torsi, N. Ditaranto, G. Tantillo, L. Ghibelli, L. Sabbatini, T. Bleve-Zacheo, M. D'Alessio, P. G. Zambonin and E. Traversa, *Chem. Mater.*, 2005, **17**, 5255–5262.

4 G. Borkow and J. Gabbay, *Curr. Chem. Biol.*, 2009, **3**, 272–278.

5 J. J. Hostynek and H. I. Maibach, *Dermatol. Ther.*, 2004, **17**, 328–333.

6 J. A. Lemire, J. J. Harrison and R. J. Turner, *Nat. Rev. Microbiol.*, 2013, **11**, 371–384.

7 H. E. Allen, T. D. Brisbin and R. H. Hall, *Environ. Sci. Technol.*, 1980, **14**, 441–443.

8 H. E. Allen and D. J. Hansen, *Water Environ. Res.*, 1996, **68**, 42–54.

9 L. A. Finney and T. V. O'Halloran, *Science (80-.).*, 2003, **300**, 931–936.

10 M. P. Murphy, *Biochem. J.*, 2009, **417**, 1–13.

11 J. Zhang, X. Wang, V. Vikash, Q. Ye, D. Wu, Y. Liu and W. Dong, *Oxid. Med. Cell. Longev.*, 2016, **2016**, 1–18.

12 S. Avery, N. Howlett and S. Radice, *Appl. Envir. Microbiol.*, 1996, **62**, 3960–3966.

13 M. Suwalsky, B. Ungerer, L. Quevedo, F. Aguilar and C. P. Sotomayor, *J. Inorg. Biochem.*, 1998, **70**, 233–238.

14 E. Baatrup, *Comp. Biochem. Physiol. Part C, Comp.*, 1991, **100**, 253–257.

15 K. L. Haas and K. J. Franz, *Chem. Rev.*, 2009, **109**, 4921–4960.

16 Z. Ma, F. E. Jacobson and D. P. Giedroc, *October*, 2009, **109**, 4644–4681.

17 K. J. Waldron, J. C. Rutherford, D. Ford and N. J. Robinson, *Nature*, 2009, 460, 823–830.

18 K. J. Waldron and N. J. Robinson, *Nat. Rev. Microbiol.*, 2009, **7**, 25–35.

19 C. Andreini, I. Bertini and A. Rosato, *Bioinformatics*, 2004, **20**, 1373–1380.

20 H. Irving and R. J. P. Williams, *J. Chem. Soc*, 1953, 3192–3210.

21 Y. Wang, E. Weisenhorn, C. W. MacDiarmid, C. Andreini, M. Bucci, J. Taggart, L. Banci, J. Russell, J. J. Coon and D. J. Eide, *metallomics*, 2018, **10**, 1755–1776.

22 L. T. Jensen, M. Ajua-Alemanji and V. C. Culotta, *J. Biol. Chem.*, 2003, **278**, 42036–42040.

23 C. W. MacDiarmid, L. A. Gaither and D. Eide, *EMBO J.*, 2000, **19**, 2845–2855.

24 L. Li, O. S. Chen, D. M. V. Ward and J. Kaplan, *J. Biol. Chem.*, 2001, **276**, 29515–29519.

25 Y. Habibi, L. A. Lucia and O. J. Rojas, *Chem. Rev.*, 2010, **110**, 3479–3500.

26 C. W. Owens, G. S. Oporto, B. C. G. Söderberg and K. E. Lambson, *J. Nanomater.*, , DOI:10.1155/2017/9461615.

27 T. Zhong, G. S. Oporto, J. Armstrong, J. Jaczynski and A. T. Tesfai, *Wood Fiber Sci.*, 2013, **45**, 215–222.

28 X. Rong-Mullins, M. J. Winans, J. B. Lee, Z. R. Lonergan, V. A. Pilolli, L. M. Weatherly, T. W. Carmenzind, L. Jiang, J. R. Cumming, G. S. Oporto and J. E. G. G. Gallagher, *Metallomics*, 2017, **9**, 1304–1315.

29 M. Hassanzadeh, R. Sabo, A. Rudie, R. Reiner, R. Gleisner and G. S. Oporto, *J. Nanomater.*, , DOI:10.1155/2017/2102987.
30 M. J. Winans, J. E. G. Gallagher, J. Jaczynski and G. Oporto, *bioRxiv*, 2019, 783076.
31 T. Zhong, G. S. Oporto, J. Jaczynski and C. Jiang, *Biomed Res. Int.*, 2015, **2015**, 456834.
32 C. Jiang, G. S. S. Oporto, T. Zhong and J. Jaczynski, *Cellulose*, 2015, **23**, 1–10.
33 K. Kasemets, A. Ivask, H. C. Dubourguier and A. Kahru, *Toxicol. Vitr.*, 2009, **23**, 1116–1122.
34 H. L. Karlsson, P. Cronholm, J. Gustafsson and L. Möller, *Chem. Res. Toxicol.*, 2008, **21**, 1726–1732.
35 K. Midander, P. Cronholm, H. L. Karlsson, K. Elihn, L. Möller, C. Leygraf and I. O. Wallinder, *Small*, 2009, **5**, 389–399.
36 S. S. V. Avery, N. N. G. Howlett and S. Radice, *Appl. Environ. Microbiol.*, 1996, **62**, 3960–3966.
37 A. Pupo, M. C. Ayers, Z. N. Sherman, R. J. Vance, J. R. Cumming and J. E. G. G. Gallagher, *Biol. Trace Elem. Res.*, 2019, 1–12.
38 L. C. Kobashigawa, Y. C. Xu, J. F. Padbury, Y. T. Tseng and N. Yano, *PLoS One*, , DOI:10.1371/journal.pone.0104888.
39 S. D. Bourque and V. I. Titorenko, *J. Vis. Exp.*, 2009, e1513.
40 A. Pupo, K. M. Ku and J. E. G. Gallagher, *PLoS One*, , DOI:10.1371/journal.pone.0223909.
41 C. A. Smith, E. J. Want, G. O'Maille, R. Abagyan, G. Siuzdak, Colin A. Smith, Elizabeth J. Want, Grace O'Maille, and Ruben Abagyan and G. Siuzdak*, - *Anal. Chem.*, 2006, **78**, 79.
42 P. Du, W. A. Kibbe and S. M. Lin, *Bioinformatics*, 2006, **22**, 2059–2065.
43 B. Zhou, J. Wang and H. W. Ressom, *PLoS One*, 2012, **7**, e40096.
44 D. S. Wishart, Y. D. Feunang, A. Marcu, A. C. Guo, K. Liang, R. Vázquez-Fresno, T. Sajed, D. Johnson, C. Li, N. Karu, Z. Sayeeda, E. Lo, N. Assempour, M. Berjanskii, S. Singhal, D. Arndt, Y. Liang, H. Badran, J. Grant, A. Serra-Cayuela, Y. Liu, R. Mandal, V. Neveu, A. Pon, C. Knox, M. Wilson, C. Manach and A. Scalbert, *Nucleic Acids Res.*, 2018, **46**, D608–D617.
45 C. Guijas, J. R. Montenegro-Burke, X. Domingo-Almenara, A. Palermo, B. Warth, G. Hermann, G. Koellensperger, T. Huan, W. Uritboonthai, A. E. Aisporna, D. W. Wolan, M. E. Spilker, H. P. Benton and G. Siuzdak, *Physiol. Behav.*, 2018, **5**, 3156–3164.
46 Q. Cui, I. A. Lewis, A. D. Hegeman, M. E. Anderson, J. Li, C. F. Schulte, W. M. Westler, H. R. Eghbalnia, M. R. Sussman and J. L. Markley, *Nat. Biotechnol.*, 2008, **26**, 162–164.
47 E. Fahy, M. Sud, D. Cotter and S. Subramaniam, *Nucleic Acids Res.*, 2007, **35**, 606–612.
48 M. Ramirez-Gaona, A. Marcu, A. Pon, A. C. Guo, T. Sajed, N. A. Wishart, N. Karu, Y. D. Feunang, D. Arndt and D. S. Wishart, *Nucleic Acids Res.*, 2017, **45**, D440–D445.
49 S. Kim, J. Chen, T. Cheng, A. Gindulyte, J. He, S. He, Q. Li, B. A. Shoemaker, P. A. Thiessen, B. Yu, L. Zaslavsky, J. Zhang and E. E. Bolton, *Nucleic Acids Res.*, 2019, **47**, D1102–D1109.
50 J. Xia, I. V. Sinelnikov, B. Han and D. S. Wishart, *Nucleic Acids Res.*, 2015, **43**, W251–W257.
51 D. J. Eide, *Biochim. Biophys. Acta - Mol. Cell Res.*, 2006, **1763**, 711–722.
52 C. A. Fierke and R. B. Thompson, *BioMetals*, 2001, **14**, 205–222.
53 J. L. Vinkenborg, M. S. Koay and M. Merkx, *Curr. Opin. Chem. Biol.*, 2010, **14**, 231–237.

54 P. J. Dittmer, J. G. Miranda, J. A. Gorski and A. E. Palmer, *J. Biol. Chem.*, 2009, **284**, 16289–16297.
55 C. Devirgiliis, C. Murgia, G. Danscher and G. Perozzi, *Biochem. Biophys. Res. Commun.*, 2004, **323**, 58–64.
56 A. Krężel and W. Maret, *Int. J. Mol. Sci.*, 2017, **18**, 1–20.
57 C. W. MacDiarmid, *EMBO J.*, 2000, **19**, 2845–2855.
58 T. W. Clarkson, *Annu. Rev. Pharmacol. Toxicol.*, 1993, 545–571.
59 C. M. Lin and D. J. Kosman, *J. Biol. Chem.*, 1990, **265**, 9194–9200.
60 C. M. Lin, B. F. Crawford and D. J. Kosman, *J. Gen. Microbiol.*, 1993, **139**, 1617–1626.
61 S. J. Stohs and D. Bagchi, *Free Radic. Biol. Med.*, 1995, **18**, 321–336.
62 M. Valko, H. Morris and M. T. D. Cronin, *Curr. Med. Chem.*, 2005, **12**, 1161–1208.
63 L. Macomber and J. A. Imlay, *Proc. Natl. Acad. Sci. U. S. A.*, 2009, **106**, 8344–8349.
64 F. F. Xu and J. A. Imlay, *Appl. Environ. Microbiol.*, 2012, **78**, 3614–3621.
65 M. Valko, C. J. Rhodes, J. Moncol, M. Izakovic and M. Mazur, *Chem. Biol. Interact.*, 2006, 160, 1–40.
66 M. Fauchon, G. Lagniel, J. C. Aude, L. Lombardia, P. Soularue, C. Petat, G. Marguerie, A. Sentenac, M. Werner and J. Labarre, *Mol. Cell*, 2002, **9**, 713–723.
67 K. Helbig, C. Grosse and D. H. Nies, *J. Bacteriol.*, 2008, **190**, 5439–5454.
68 K. Helbig, C. Bleuel, G. J. Krauss and D. H. Nies, *J. Bacteriol.*, 2008, **190**, 5431–5438.
69 Y. Zhao, P. K. K. Strope, S. G. G. Kozmin, J. H. H. McCusker, F. S. S. Dietrich, R. J. J. Kokoska and T. D. D. Petes, *G3 (Bethesda).*, 2014, **4**, 2259–2269.
70 M. Karin, R. Najarian, A. Haslinger, P. Valenzuela, J. Welch, S. Fogel, R. Najariant, A. Haslinger, P. Valenzuelat and J. Welcht, *Proc Natl Acad Sci U S A*, 1984, **81**, 337–341.
71 B. N. Ames and L. S. Gold, *Mutat. Res. - Fundam. Mol. Mech. Mutagen.*, 1991, **250**, 3–16.
72 B. Halliwell and O. I. Aruoma, *Fed. Eur. Biochem. Soc.*, 1991, **281**, 9–19.
73 G. G. Perrone, S. X. Tan and I. W. Dawes, *Biochim. Biophys. Acta - Mol. Cell Res.*, 2008, **1783**, 1354–1368.
74 F. Madeo, E. Fröhlich, M. Ligr, M. Grey, S. J. Sigrist, D. H. Wolf, K. Fröhlich, P. Institut, U. Tübingen, A. Institut, I. Biochemie, U. Stuttgart, W. Goethe-universität and F. Main, 1999, **145**, 757–767.
75 Q. Liang and B. Zhou, *Mol. Biol. Cell*, 2007, **18**, 4741–9.
76 F. Madeo, E. Fröhlich and K. U. Fröhlich, *J. Cell Biol.*, 1997, **139**, 729–734.
77 R. Reekmans, K. De Smet, C. Chen, P. Van Hummelen and R. Contreras, *FEMS Yeast Res.*, 2005, **5**, 711–725.
78 W. Jian, J. S. Arora, T. Oe, V. V. Shuvaev and I. A. Blair, *Free Radic. Biol. Med.*, 2005, **39**, 1162–1176.
79 B. Zhivotovsky and G. Kroemer, *Nat. Rev. Mol. Cell Biol.*, 2004, **5**, 752–762.
80 W. A. Pryor, *Free Radic. Biol. Med.*, 1989, **7**, 177–178.
81 H. Esterbauer and K. H. Cheeseman, *Methods Enzymol.*, 1990, **186**, 407–421.
82 A. Ayala, M. F. Muñoz and S. Argüelles, *Oxid. Med. Cell. Longev.*, 2014, 1–31.
83 H. Yin, L. Xu and N. A. Porter, *Chem. Rev.*, 2011, **111**, 5944–5972.
84 A. W. Girotti, *J. Lipid Res.*, 1998, **39**, 1529–1542.
85 M. V. Evans, H. E. Turton, C. M. Grant and I. W. Dawes, *J. Bacteriol.*, 1998, **180**, 483–490.
86 A. Negre-Salvayre, C. Coatrieux, C. Ingueneau and R. Salvayre, *Br. J. Pharmacol.*, 2008,

153, 6–20.
87 B. Halliwell and J. M. C. Gutteridge, *Biochem. J.*, 1984, **219**, 1–14.
88 M. Slaba, P. Bernat, S. Rózalska, J. Nykiel and J. Długoński, *Acta Biochim. Pol.*, 2013, **60**, 695–700.
89 M. F. Renne and A. I. P. M. de Kroon, *FEBS Lett.*, 2018, **592**, 1330–1345.
90 D. Toomre, K. Simons and D. Toomre, *Nat. Rev. Mol. Cell Biol.*, 2000, **1**, 1.
91 G. Van Meer, D. R. Voelker and G. W. Feigenson, *Nat. Rev. Mol. Cell Biol.*, 2008, **9**, 112–124.
92 O. Tehlivets, K. Scheuringer and S. D. Kohlwein, *Biochim. Biophys. Acta - Mol. Cell Biol. Lipids*, 2007, **1771**, 255–270.
93 D. Ackerman, S. Tumanov, B. Qiu, E. Michalopoulou, M. Spata, A. Azzam, H. Xie, M. C. Simon and J. J. Kamphorst, *Cell Rep.*, 2018, **24**, 2596-2605.e5.
94 T. Eisenberg and S. Büttner, *FEMS Yeast Res.*, 2014, **14**, 179–197.
95 T. Czabany, K. Athenstaedt and G. Daum, *Biochim. Biophys. Acta - Mol. Cell Biol. Lipids*, 2007, **1771**, 299–309.
96 A. Wolf, P. Weir, P. Segar, J. Stone and J. Shield, *Lancet*, 2001, **357**, 606–607.
97 R. Santer, R. Fingerhut, U. Lässker, P. J. Wightman, D. R. Fitzpatrick, B. Olgemöller and A. A. Roscher, *Clin. Chem.*, 2003, **49**, 660–662.
98 N. Napolitano, V. Wiley and J. J. Pitt, *J. Inherit. Metab. Dis.*, 2004, **27**, 465–471.
99 A. Rötig and A. Munnich, *J. Am. Soc. Nephrol.*, 2003, **14**, 2995–3007.
100 J. R. Harris and E. J. (Eds. . Boekema, *Membrane Protein Complexes: Structure and Function*, 2018, vol. 87.
101 P. A. A. Cobine, L. D. D. Ojeda, K. M. M. Rigby and D. R. R. Winge, *J. Biol. Chem.*, 2004, **279**, 14447–14455.
102 S. C. Leary, D. R. Winge and P. A. Cobine, *Biochim. Biophys. Acta - Mol. Cell Res.*, 2009, **1793**, 146–153.
103 V. V. Mossine and T. P. Mawhinney, *1-Amino-1-deoxy-d-fructose ('Fructosamine') and its Derivatives*, 2010, vol. 64.
104 V. V. Mossine and T. P. Mawhinney, *J. Agric. Food Chem.*, 2007, **55**, 10373–10381.
105 B. Gyurcsik, T. Gajba, L. Nagy, K. Burger, A. Rockenbauer and L. Korecz, *Inorganica Chim. Acta*, 1993, **1**, 57–66.
106 A. Naranuntarat, L. T. Jensen, S. Pazicni, J. E. Penner-Hahn and V. C. Culotta, *J. Biol. Chem.*, 2009, **284**, 22633–22640.
107 L. M. Buu, Y. C. Chen and F. J. S. Lee, *J. Biol. Chem.*, 2003, **278**, 17203–17209.
108 P. McGraw and S. A. Henry, *Genetics*, 1989, **122**, 317–330.
109 I. D. Schlatter, M. Meira, V. Ueberschlag, D. Hoepfner, R. Movva and N. E. Hynes, *PLoS One*, , DOI:10.1371/journal.pone.0032501.
110 A. M. Avery and S. V. Avery, *J. Biol. Chem.*, 2001, **276**, 33730–33735.
111 M. J. Kuranda and P. W. Robbins, *J. Biol. Chem.*, 1991, **266**, 19758–19767.
112 C. O'Conalláin, M. T. Doolin, C. Taggart, F. Thornton and G. Butler, *Mol. Gen. Genet.*, 1999, **262**, 275–282.
113 C. Cappellaro, V. Mrsa and W. Tanner, *J. Bacteriol.*, 1998, **180**, 5030–5037.
114 Y. Luo, J. Wang, B. Liu, Z. Wang, Y. Yuan and T. Yue, *PLoS One*, , DOI:10.1371/journal.pone.0136045.
115 S. Vijayarathna, Z. Zakaria, Y. Chen, L. Y. Latha, J. R. Kanwar and S. Sasidharan, *Molecules*, 2012, **17**, 4860–4877.

116 S. L. Jothy, Z. Zakariah, Y. Chen and S. Sasidharan, *Molecules*, 2012, **17**, 6997–7009.
117 F. Z. Idrissi, A. Blasco, A. Espinal and M. I. Geli, *Proc. Natl. Acad. Sci. U. S. A.*, , DOI:10.1073/pnas.1202789109.
118 C. Buser and D. G. Drubin, *Microsc Microanal*, 2013, **19**, 381–392.
119 I. K. Jarsch, F. Daste and J. L. Gallop, *J. Cell Biol.*, 2016, **214**, 375–387.
120 A. A. Duina, M. E. Miller and J. B. Keeney, *Genetics*, 2014, **197**, 33–48.
121 E. Nikko and H. R. B. Pelham, *Traffic*, 2009, **10**, 1856–1867.
122 E. Nikko, J. A. Sullivan and H. R. B. Pelham, *EMBO Rep.*, 2008, **9**, 1216–1221.
123 C. H. Lin, J. A. MacGurn, T. Chu, C. J. Stefan and S. D. Emr, *Cell*, 2008, **135**, 714–725.
124 D. C. Prosser, A. E. Pannunzio, J. L. Brodsky, J. Thorner, B. Wendland and A. F. O'Donnell, *J. Cell Sci.*, 2015, **128**, 4220–4234.
125 W. Kukulski, M. Schorb, M. Kaksonen and J. A. G. Briggs, *Cell*, 2012, **150**, 508–520.
126 M. E. Letelier, A. M. Lepe, M. Faúndez, J. Salazar, R. Marín, P. Aracena and H. Speisky, *Chem. Biol. Interact.*, 2005, **151**, 71–82.